PROCEEDINGS OF THE ROYAL SOCIETY A MATHEMATICAL, PHYSICAL & ENGINEERING SCIENCES

Propagation in waveguides with varying cross section and curvature: a new light on the role of supplementary modes in multi-modal methods

Agnès Maurel, Jean-François Mercier and Simon Félix

Proc. R. Soc. A 2014 **470**, 20140008, published 9 April 2014

PROCEEDINGS OF THE ROYAL SOCIETY A

rspa.royalsocietypublishing.org

Propagation in waveguides with varying cross section and curvature: a new light on the role of supplementary modes in multi-modal methods

Agnès Maurel[1], Jean-François Mercier[2] and Simon Félix[3]

[1]Institut Langevin, CNRS, ESPCI ParisTech, 1 rue Jussieu, Paris 75005, France

[2]Poems, CNRS, ENSTA ParisTech, INRIA, 828 boulevard des Maréchaux, Palaiseau 91762, France

[3]LAUM, CNRS, Université du Maine, Avenue Olivier Messiaen, Le Mans 72085, France

Research

Cite this article: Maurel A, Mercier J-F, Félix S. 2014 Propagation in waveguides with varying cross section and curvature: a new light on the role of supplementary modes in multi-modal methods. *Proc. R. Soc. A* **470**: 20140008.
http://dx.doi.org/10.1098/rspa.2014.0008

Received: 4 January 2014
Accepted: 10 March 2014

Subject Areas:
acoustics, mathematical physics

Keywords:
waveguide, multi-modal method, boundary mode, admittance matrix

Author for correspondence:
Agnès Maurel
e-mail: agnes.maurel@espci.fr

We present an efficient multi-modal method to describe the acoustic propagation in waveguides with varying curvature and cross section. A key feature is the use of a flexible geometrical transformation to a virtual space in which the waveguide is straight and has unitary cross section. In this new space, the pressure field has to satisfy a modified wave equation and associated modified boundary conditions. These boundary conditions are in general not satisfied by the Neumann modes, used for the series representation of the field. Following previous work, an improved modal method (MM) is presented, by means of the use of two supplementary modes. Resulting increased convergences are exemplified by comparison with the classical MM. Next, the following question is addressed: when the boundary conditions are verified by the Neumann modes, does the use of supplementary modes improve or degrade the convergence of the computed solution? Surprisingly, although the supplementary modes degrade the behaviour of the solution at the walls, they improve the convergence of the wavefield and of the scattering coefficients. This sheds a new light on the role of the supplementary modes and opens the way for their use in a wide range of scattering problems.

Royal Society Publishing

1. Introduction

Guided waves have a wide range of applications in engineering and physics and they have been subjected to investigation for many years in the context of electromagnetic [1,2], acoustic [3,4] and elastic [5,6] waveguides as well as in the context of shallow oceans [7–9]. For uniform and infinite waveguides, separation of variables is possible and exact solutions of the guided wave propagation (modes) exist. However, when longitudinal variations occur, the separability is in general lost.

Modal methods (MMs) consist in using the set of modes of the uniform waveguide for the series representation of the wavefield. This has the advantage of recovering simple solutions outside the non-uniform regions of the waveguide, where the modes are exact solutions. The numerical scheme has to describe the mode coupling inside the scattering regions accounting for the radiation and source conditions. These multi-modal methods have been shown to be computationally efficient in several contexts [10–12]. Efficient is meant here notably as: energy conservation and reciprocity are preserved and high convergence is obtained with respect to the number of modes used in the series representation. This high convergence can be understood, when compared with the highest possible convergence of the wavefield. Indeed, when truncating a series, say $p = \sum_{n=0}^{N-1} p_n \varphi_n$, the best convergence that can be expected is limited by the weight, or the error, of the remaining series, namely $\sum_{n=N}^{\infty} p_n \varphi_n$, and this error can be theoretically evaluated by inspecting the general term p_n of the series. Note also that, outside the scattering region, the remaining series has an exponential decrease (given by the evanescent modes p_n), and thus the convergence is given by the behaviour of the propagating modes for which no theoretical results exist. This gives the convergence of the scattering coefficients (the reflection and transmission coefficients) that will be considered in this paper.

In several situations, it turns out that the high convergences of MMs are lost (see table 1, which summarizes previous results and anticipates the results obtained in this paper). The reason is well identified: if the scattering region produces a change in the boundary conditions, each mode does not satisfy the right condition at the walls, and the solution, being a finite superposition of modes, behaves the same. This is the price to pay and let us give an example: consider a waveguide with Neumann boundary conditions on the walls and with local curvature but constant cross section (second row in table 1). In the scattering regions, the modes satisfy the right boundary condition (vanishing first derivative), resulting in a close to N^{-3} convergence of the wavefield [12]. If, in addition, a variable cross section is considered, the modes do not satisfy the boundary condition of the vanishing normal derivative, resulting in a decrease in the convergence close to N^{-1} (third row of table 1; see [12]). In previous papers, Athanassoulis & Belibassakis [14,15] propose to enrich the set of modes used for the series representation; see also [16,17]. The supplementary mode, also called the boundary mode in those papers, is chosen with a non-zero first derivative and this is thought to be able to restore the right boundary condition. Although not guaranteed *a priori*, it has been shown that this enriched set of modes restores the highest $N^{-7/2}$ convergence in at least two circumstances: for waveguides with varying cross section [13,17] and for waveguides with Robin boundary condition [18]. Moreover, a superconvergence of the scattering coefficients has been reported in [13], from $1/N$ without boundary mode to $1/N^{4.5}$ with a supplementary boundary mode (first row of table 1).

In this paper, we consider the acoustic propagation in a two-dimensional waveguide with variable cross section and curvature. As in [13,17], the presented improved modal method (IMM) aims at a consistent numerical scheme with high convergence and this will be done by comparison with the classical MM, as used in [12]. Also, the goal is to revisit the role of the supplementary modes with respect to the convergence of the wavefield inside the scattering region and the scattering coefficients. This will be done by considering the particular configuration of the serpent billiard. Indeed, this geometry can be treated by considering either a constant cross section and varying curvature, or a varying cross section and zero curvature. If variable cross section is considered, the Neumann modes used in the MM cannot satisfy the right boundary conditions at the walls, and the IMM has improved convergences compared with the MM, as expected (first

Table 1. Convergences of the wavefield (WF) without and with the supplementary mode (SM, in second and third columns) and convergences of the reflection coefficients (R) without and with the supplementary mode (fourth and fifth columns).

	WF without SM	WF with SM	R without SM	R with SM
h variable, $\kappa = 0$, from [13]	$1/N$	$1/N^{3.5}$	$1/N$	$1/N^{4.5}$
present work	$1/N$	$1/N^{3.5}$	$1/N$	$1/N^{5}$
h constant, $\kappa \neq 0$, from [12]	$1/N^{3.2\pm0.1}$			
present work	$1/N^{3}$	$1/N^{3.5}$	$1/N^{3}$	$1/N^{5}$
h variable, $\kappa \neq 0$, from [12]	$1/N^{2\pm0.5}$			
present work	$1/N$	$1/N^{3.5}$	$1/N^{3.5}$	$1/N^{5.5}$

row of table 1). If variable curvature is considered, one can build the Neumann modes of the MM such that they satisfy the right condition of vanishing normal derivatives at the walls. In this case, the classical MM has a good convergence, as observed in [12], and, in fact, one could think that adding modes that do not satisfy this condition will make it worse. *De facto*, the normal derivative of the solution is non-zero at the walls in the IMM and one finds that it vanishes asymptotically only, for large truncation N (in $1/N^2$). Nevertheless, one observes that both convergences, of the pressure field and scattering coefficients, are increased (second row of table 1). This means that the virtue of the supplementary mode is not, or not only, to restore the right boundary condition.

The paper is organized as follows. In §2, we use the geometrical transformation to derive the modified wave equation, written in a 'virtual' straight waveguide, equation (2.8), and associated modified boundary conditions, (2.9). The transformation is chosen for its flexibility, which renders the presented method accessible to a large class of waveguide geometry. In previous studies [19–22], angle-preserving transformations (as conformal mapping) were preferred, and this is discussed. Next, in §3, the multi-modal formulation is derived, equation (3.3). This is done by expanding the solution onto a set of transverse functions (the modes), assumed to verify specified orthogonality relations, equations (3.2). The choice of the transverse functions in the MM and in the IMM is discussed in §3*b*. In §4, we first validate our multi-modal method in the geometry of the 'elephant's trunk', already considered in [12]. The improvement of the IMM is confirmed, for the convergences both of the wavefield and of the reflection coefficients (row 3 of table 1). Then, we consider the geometry of the serpent billiard. Two different choices for the geometrical transformation are presented, leading to (i) zero curvature and a varying cross section or (ii) varying curvature and a constant cross section. In the former case (i), the improvement in the convergences in the IMM is confirmed, as expected (first row in table 1). In the latter case (ii), the IMM is shown to be again more efficient than the MM (second row of table 1), although the computed wavefield does not satisfy the right boundary condition at the walls.

We have collected in the appendices useful calculations. In appendix A, the properties of the numerical schemes, in terms of the reciprocity and the energy conservation, are discussed. In appendix B, we give elements on the numerical implementation of the multi-modal methods and the calculation of the errors as used for the presented results. Finally, in appendix C, the explicit expressions of the matrices used in the MM and IMM are given.

2. Modified wave equations and boundary conditions

In this section, we use a geometrical transformation, from the direct space, (x, y), to a new space, (X, Y), in which the waveguide has a straight axis and a constant and unitary cross section. The resulting modified wave equation (2.8) and associated modified boundary conditions (2.9) are derived.

Consider a two-dimensional waveguide Ω, defined by the boundaries $\mathbf{S_1}(x, y)$ (lower wall $\mathbf{C_1}$) and $\mathbf{S_2}(x, y)$ (upper wall $\mathbf{C_2}$) (figure 1). In the frequency regime, assuming an inviscid

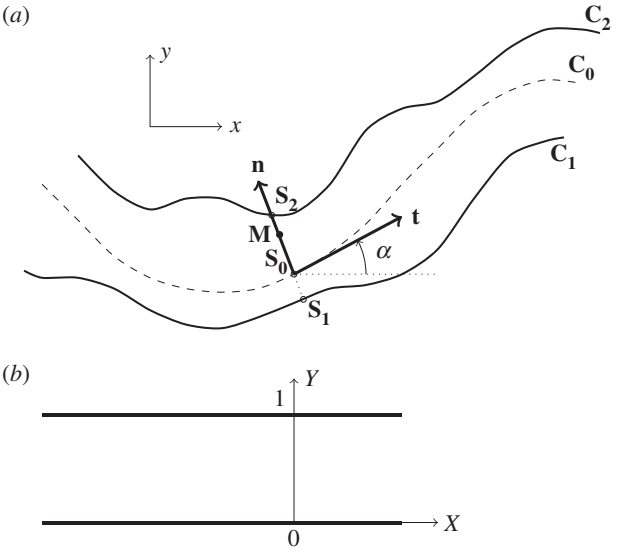

Figure 1. (*a*) Geometry of the waveguide with varying curvature and cross section in the direct (x, y) space. (*b*) Resulting configuration after geometrical transformation in the new (X, Y) space.

homogeneous medium filling the waveguide, the pressure field satisfies the wave propagation problem

$$(\Delta + k^2)p = 0 \quad \text{in } \Omega \tag{2.1}$$

and

$$\mathbf{N}_i \cdot \nabla p = 0 \quad \text{on } \mathbf{C_i}, \quad i = 1, 2, \tag{2.2}$$

with $\mathbf{N}_i$ the normal to the boundary.

To begin with, we define a reference axis $\mathbf{C_0}$, described by the function $\mathbf{OS_0}(X)$, and X is the arc length along $\mathbf{C_0}$ (obviously, the choice of $\mathbf{C_0}$ is not unique, and this will be illustrated in §4*b*). Then, the boundaries $\mathbf{C_1}$ and $\mathbf{C_2}$ are parametrized as, respectively,

$$\mathbf{OS_1}(X) = \mathbf{OS_0}(X) + h_1(X)\,\mathbf{n}(X)$$

and

$$\mathbf{OS_2}(X) = \mathbf{OS_0}(X) + h_2(X)\,\mathbf{n}(X),$$

where $\mathbf{n}$ is the normal component of the local Frenet–Serret frame $(\mathbf{t}, \mathbf{n})$,

$$\frac{\mathrm{d}\mathbf{OS_0}}{\mathrm{d}X} = \mathbf{t} \quad \text{and} \quad \frac{\mathrm{d}\mathbf{n}}{\mathrm{d}X} = -\kappa(X)\mathbf{t},$$

and κ is the local curvature of $\mathbf{C_0}$. For $\mathbf{M}(x, y)$ a point in Ω, we use the change of variable $(x, y) \to (X, Y)$, with Y a local coordinate associated with the normal vector $\mathbf{n}$. Thus,

$$\mathbf{OM} = x\mathbf{i} + y\mathbf{j} = \mathbf{OS_0}(X) + g(X, Y)\mathbf{n}(X),$$

with

$$g(X, Y) \equiv h_1(X) + Yh(X),$$

$h(X) \equiv h_2(X) - h_1(X)$ being the local width of the waveguide, and $Y \in [0, 1]$. Then,

$$\mathrm{d}\mathbf{OM} = \mathrm{d}x\mathbf{i} + \mathrm{d}y\mathbf{j} = [(1 - \kappa g)\mathbf{t} + g'\mathbf{n}]\,\mathrm{d}X + h\mathbf{n}\,\mathrm{d}Y,$$

from which we deduce the Jacobian J^{-1} of the transformation $(X, Y) \to (x, y)$,

$$\begin{pmatrix} \partial_X \\ \partial_Y \end{pmatrix} = \mathbf{J}^{-1} \begin{pmatrix} \partial_x \\ \partial_y \end{pmatrix}, \quad \text{with } \mathbf{J}^{-1} = \begin{pmatrix} f & g' \\ 0 & h \end{pmatrix} R_{-\alpha}.$$

Here, g' stands for $\partial_X g$, and the function f is defined by

$$f \equiv (1 - \kappa g),$$

and R_α is the rotation matrix of angle α (figure 1), with $\alpha'(X) = \kappa(X)$. The wave equation in (X, Y) then reads as

$$\nabla \cdot (\mathtt{H}\nabla p) + \frac{k^2}{\det \mathtt{J}} p = 0, \quad \text{with } \mathtt{H} \equiv \frac{{}^t\mathtt{J}\,\mathtt{J}}{\det \mathtt{J}}, \tag{2.3}$$

and with the boundary conditions

$$[\mathtt{H}\nabla p]_{Y=0,1} \cdot \mathbf{e}_Y = 0, \tag{2.4}$$

with $\mathbf{e}_Y = {}^t(0, 1)$.

Let us comment on the chosen transformation. Its main advantage lies in its flexibility. Although it is not guaranteed that any waveguide geometry makes possible the choice of C_0 to produce a proper mesh (for instance, one needs $(1 - \kappa g) \neq 0$; see [16]), most of the geometries can be treated easily. In addition, it is straightforward to extend it to three-dimensional geometries. Its disadvantage is that it modifies in general both the structure of the Helmholtz equation and the boundary condition, because the matrix $\mathtt{H} \equiv {}^t\mathtt{J}\mathtt{J}/\det \mathtt{J}$ is not diagonal

$$\mathtt{H} = \begin{pmatrix} \dfrac{h}{f} & -\dfrac{g'}{f} \\ -\dfrac{g'}{f} & \dfrac{f^2 + g'^2}{hf} \end{pmatrix}, \tag{2.5}$$

and this is why we will use supplementary modes. In the case of orthogonal transformations, $\partial_x X \partial_x Y + \partial_y X \partial_y Y = 0$, $\mathtt{H}$ is diagonal, which ensures that the boundary condition $\partial_n p_{|\text{walls}} = 0$ becomes $\partial_Y p(X, Y = 0, 1) = 0$ (the transformation is angle preserving); such a transformation has been proposed in [21,23]. Although they remain valid for many configurations, they require an iterative, numerical, process to get the local coordinate, which may be involved. Alternatively, conformal mappings have been proposed [19,20] which ensure $\partial_x X = \partial_y Y$ and $\partial_x Y = -\partial_y X$ (the Cauchy–Riemann conditions for holomorphic transformations). Thus, $\mathtt{H} = \mathtt{I}$, which means that (i) the transformation is orthogonal and (ii) the structure of the Helmholtz equation is preserved, that is, the wavefield satisfies $\Delta p + (k^2/\det \mathtt{J})p = 0$, which describes wave propagation in a medium with variable index. Finally, it is a generalization of the transformation used in [22,24] for varying curvature but a constant cross section. In this case, the natural curvilinear coordinates are $(X, \xi = hY)$ with constant h and $h_1 = 0$, thus $g' = 0$ and $f = 1 - \kappa\xi$, and

$$\mathtt{H} = \begin{pmatrix} \dfrac{h}{1 - \kappa\xi} & 0 \\ 0 & \dfrac{1 - \kappa\xi}{h} \end{pmatrix}, \tag{2.6}$$

leading to the second-order eqn (3) in [22] and eqn (2.3) in [24].

In the following, we rewrite the second-order equation (2.3) in terms of two coupled first-order equations. To do that, we introduce a new field $q(X, Y)$ related to $p(X, Y)$. The field q is chosen inspecting equation (2.3)

$$q(X, Y) = \frac{1}{f}(h\partial_X p - g'\partial_Y p), \tag{2.7}$$

which leads to a reformulation of equation (2.3)

$$\frac{\partial}{\partial X}\begin{pmatrix} p \\ q \end{pmatrix} = \begin{pmatrix} \dfrac{g'}{h}\partial_Y & \dfrac{f}{h} \\ -\partial_Y\left(\dfrac{f}{h}\partial_Y\right) - fk^2 h & \partial_Y\left(\dfrac{g'}{h}.\right) \end{pmatrix}\begin{pmatrix} p \\ q \end{pmatrix}, \tag{2.8}$$

and the boundary conditions, equation (2.4), are $[-hg'\partial_X p + (g'^2 + f^2)\partial_Y p]_{Y=0,1} = 0$, that is, using equation (2.7) to eliminate $\partial_X p$,

$$[f\partial_Y p - g'q]_{Y=0,1} = 0. \tag{2.9}$$

In §3, we project equation (2.8), using equation (2.9), onto a set of transverse functions $\varphi_n(Y)$ that will be defined in the MM and the IMM.

3. Modal formulation

(a) Projection of the wave equation

We now use the modal decompositions for the fields p and q

$$\left.\begin{aligned} p(X,Y) &= \sum_n p_n(X)\varphi_n(Y) \\ \text{and} \qquad q(X,Y) &= \sum_n q_n(X)\varphi_n(Y), \end{aligned}\right\} \tag{3.1}$$

where (φ_n) is a set of transverse functions chosen to fulfil the orthogonality relations

$$\left.\begin{aligned} (\varphi_m, \varphi_n) &= \delta_{mn} \\ \text{and} \qquad (\varphi'_m, \varphi'_n) &= \gamma_m^2 \delta_{mn}, \end{aligned}\right\} \tag{3.2}$$

with $(f,g) \equiv \int_0^1 \bar{f} g \, \mathrm{d}Y$ the scalar product and $\bar{f}$ the complex conjugate (the choice of these transverse functions is discussed in the following). The projection of the coupled evolution equation (2.8), accounting for the boundary conditions (2.9), then leads to a new set of coupled equations governing the variations along X of the vectors $\mathbf{p} \equiv (p_n)$ and $\mathbf{q} \equiv (q_n)$,

$$\frac{\mathrm{d}}{\mathrm{d}X}\begin{pmatrix}\mathbf{p}\\ \mathbf{q}\end{pmatrix} = \frac{1}{h}\begin{pmatrix} h'\mathsf{E} + h_1'\mathsf{F} & (1-\kappa h_1)\mathsf{I} - \kappa h\mathsf{C} \\ (1-\kappa h_1)\mathsf{K}^2 + \kappa h[(kh)^2\mathsf{C} - \mathsf{D}] & -{}^t(h'\mathsf{E} + h_1'\mathsf{F}) \end{pmatrix}\begin{pmatrix}\mathbf{p}\\ \mathbf{q}\end{pmatrix}, \tag{3.3}$$

where I is the identity matrix and

$$\left.\begin{aligned} \mathsf{C}_{mn} \equiv (Y\varphi_m, \varphi_n), \quad \mathsf{D}_{mn} \equiv (Y\varphi'_m, \varphi'_n), \quad \mathsf{E}_{mn} \equiv (Y\varphi_m, \varphi'_n), \\ \mathsf{F}_{mn} \equiv (\varphi_m, \varphi'_n) \quad \text{and} \quad \mathsf{K}_{mn} \equiv \mathrm{j}\sqrt{(kh)^2 - \gamma_m^2}\delta_{mn} = \mathrm{j}k_n h. \end{aligned}\right\} \tag{3.4}$$

It is straightforward to see that the properties of reciprocity and energy conservation are preserved in the above formulation (see details in appendix A).

The above system, equation (3.3), has another important property: in the straight parts of the guide, say at the input and output ends where h is constant, the system is decoupled, with $p'_n = q_n/h$ and $q'_n/h = -k_n^2 p_n$. This leads to the expected behaviour $p_n \propto \mathrm{e}^{\pm \mathrm{i}k_n X}$ in these parts, which can be used to translate the radiation condition and this is essential for the numerical implementation ([13]; see also appendix B).

Finally, equation (3.3) has been derived assuming that the transverse functions satisfy the relations in equations (3.2). This is true for the classical transverse functions of the Neumann problem and it will be shown in §3*b* how to build the supplementary modes in the IMM to preserve them.

(b) Transverse functions in the modal method and improved modal method

For waveguides with Neumann boundary conditions on the walls, the functions φ_n are chosen as the solutions of the transverse eigenproblem

$$\varphi_n'' = -\gamma_n^2 \varphi_n, \tag{3.5}$$

with the boundary condition $\varphi_n' = 0$ at the walls ($Y = 0, 1$). In the two-dimensional case under study, these modes are

$$\varphi_n(Y) = \sqrt{2 - \delta_{n0}}\cos(n\pi Y),$$

with the eigenvalues $\gamma_n = n\pi$. However, the varying cross section and curvature may produce boundary conditions, equation (2.9), that are not satisfied by the φ_n. Strictly, the expansion of p onto the infinite set of φ_n, equation (3.1), is possible because the φ_n forms a complete basis, and this has been done in [12,25]. However, numerical computations involve truncated series, which then become inconsistent with the boundary condition because each transverse mode violates it. Because the computed solution is a superposition of modes, it behaves in the same way, resulting in a poor convergence of the numerical method.

Following [13,17], we consider supplementary modes thought to be able to restore the right boundary conditions. In principle, it is sufficient to consider any supplementary functions $\chi(Y)$ with non-zero derivatives at $Y = 0, 1$, as done in [14–16,26,27]. However, if the set of classical Neumann $\{\varphi_n\}_{n\in\mathbb{N}}$ satisfies the desired orthogonality relations equations (3.2), it is in general not the case if one includes a supplementary function. To ensure that the orthogonality relations are satisfied, and following [13,17], the MM is improved by introducing two supplementary modes, built from two χ_1 and χ_2, but rearranged to satisfy the desired properties. These are

$$\varphi_{-i}(Y) \equiv a_{iN}\left(\chi_i(Y) - \sum_{n=0}^{N-1} \chi_{in}\varphi_n(Y)\right), \quad i = 1, 2, \tag{3.6}$$

where $\chi_{in} \equiv (\varphi_n, \chi_i)$ and a_{iN} are normalization coefficients (note that, in [13], the a_{iN} are included in the definition of χ_i; here, χ_i is a function independent of N).

In the case of a single boundary mode, the above definition would be sufficient to ensure equations (3.2). Indeed, φ_{-i} is orthogonal to all $\varphi_{n\geq 0}$ by construction, and we have also $(\varphi_{-i}', \varphi_{n\geq 0}') = -(\varphi_{-i}, \varphi_{n\geq 0}'') = 0$, because $\varphi_{n\geq 0}'' = -\gamma_n^2\varphi_n$. For two supplementary functions, one has also to ensure that $(\varphi_{-1}, \varphi_{-2}) = (\varphi_{-1}', \varphi_{-2}') = 0$ and this is not straightforward. Indeed, we have

$$\left.\begin{aligned} (\varphi_{-1}, \varphi_{-2}) &= a_{1N}a_{2N}\left[(\chi_1, \chi_2) - \sum_{n=0}^{N-1} \chi_{1n}\chi_{2n}\right] \\ \text{and} \quad (\varphi_{-1}', \varphi_{-2}') &= a_{1N}a_{2N}\left[(\chi_1', \chi_2') - \sum_{n=0}^{N-1} \gamma_n^2\chi_{1n}\chi_{2n}\right], \end{aligned}\right\} \tag{3.7}$$

and we want these quantities to vanish for any truncation N. This implies $(\chi_1, \chi_2) = (\chi_1', \chi_2') = 0$ (say, for $N = 1$) and thus, also, $\chi_{1n}\chi_{2n} = 0$ for any n. With $\varphi_{n\geq 0}$ being either symmetric functions (n even) or antisymmetric functions (n odd), the easiest way to ensure $(\chi_1, \chi_2) = (\chi_1', \chi_2') = 0$ and $\chi_{1n}\chi_{2n} = 0$ for any n is to build a symmetric χ_1 and an antisymmetric χ_2. That way, both the functions (χ_1, χ_2) and their derivatives are orthogonal; also, the projection of χ_1 on an antisymmetric φ_n vanishes and the projection of χ_2 on a symmetric φ_n vanishes. This produces $\chi_{1n}\chi_{2n} = 0$ for any n. In the present case, this is possible by defining

$$\left.\begin{aligned} \chi_1(Y) &= a_1\left[\cos\left(\frac{\pi Y}{2}\right) + \sin\left(\frac{\pi Y}{2}\right)\right] \\ \text{and} \quad \chi_2(Y) &= a_2\left[\cos\left(\frac{\pi Y}{2}\right) - \sin\left(\frac{\pi Y}{2}\right)\right], \end{aligned}\right\}$$

where $a_1 = 1/\sqrt{1 + 2/\pi}$ and $a_2 = 1/\sqrt{1 - 2/\pi}$ are normalization factors such that $(\chi_i, \chi_i) = 1$, as in [17]. However, note that the constraints on the χ_i functions may be penalizing depending on the

role that is demanded of the supplementary modes. The new set of transverse functions $\{\varphi_n\}$, $n \in [-2, N-1]$, fulfils the orthogonality relations (3.2), with the normalization factors

$$a_{iN} = \left[1 - \sum_{n=0}^{N-1} \chi_{in}^2\right]^{-1/2} \quad \text{and} \quad \gamma_{-i}^2 = \frac{\beta_i^2 - \sum_{n=0}^{N-1} \chi_{in}^2 (n\pi)^2}{1 - \sum_{n=0}^{N-1} \chi_{in}^2}, \quad i = 1, 2,$$

where $\beta_1 = a_1\pi/2a_2$ and $\beta_2 = a_2\pi/2a_1$. Thus, with or without the supplementary modes, the first-order matrix evolution equation governing $\mathbf{p}$ and $\mathbf{q}$ keeps exactly the same form (3.3) and the definitions of matrices C, D, E and F remain unchanged (these matrices are given in appendix C).

4. Results

In this section, we inspect the accuracy and convergences of the IMM when compared with the classical method, MM. This is done firstly in a reference configuration, the so-called 'elephant's trunk', already considered in [12] using the MM. Next, we consider the configuration of the serpent billiard that allows for two different geometrical transformations. The former example is used to inspect the computational efficiency of the improved method while the second example sheds a new light on the role of the supplementary modes.

Before we begin, let us mention some technical points:

(i) The error on the wavefield is classically defined as

$$\epsilon_N \equiv \frac{\|p^N - p^e\|}{\|p^e\|}, \tag{4.1}$$

with $\|a\| \equiv [\int \mathrm{d}x\,\mathrm{d}y |a(x,y)|^2]^{1/2}$, and, in the definition above, $p^N \equiv \sum_{n=0}^{N-1} p_n \varphi_n$ is the field computed with a series truncated at order N and p^e refers to an exact solution, in practice computed with a high N_e truncation. We also consider the error on the reflection coefficient R of the mode 0 (for an incident mode 0), simply defined as

$$\epsilon_N^R \equiv \frac{|R^N - R^e|}{|R^e|}. \tag{4.2}$$

In the MM, the error on the wavefield is more accurately calculated owing to

$$\|p^N(x,y) - p^e(x,y)\|^2 = \sum_{n=0}^{N-1} \int \mathrm{d}x |p_n^e - p_n^N|^2 + \sum_{n=N}^{N_e} \int \mathrm{d}x |p_n^e|^2.$$

The first sum evaluates the error on the modal component p_n^N for increasing N value and the second sum is a truncated version of the remaining series (obtained assuming that the coefficients p_n are independent of the truncation N). This simple calculation uses the orthogonality of the φ_n. In the IMM, φ_{-1} is orthogonal to φ_n for $0 \le n \le N-1$ but not to $\varphi_{n>N}$, so the calculation of the error is more involved, and we give in appendix B*a* the expression we have used in the presented results, equations (B 7) and (B 8).

(ii) As previously stated, the convergence ϵ_N of the wavefield is limited to the weight of the remaining series, and this weight can be evaluated by inspecting the general term of the series. This is because $|p_n| \propto n^{-a}$ produces $[\sum_{n=N}^{\infty} \int \mathrm{d}x |p_n^e|^2]^{1/2} \propto N^{-a+1/2}$. In the MM formulation, the general term in the expansion equation (3.1) is simply p_n. But in the IMM formulation, the supplementary modes φ_{-1} and φ_{-2} also depend on the truncation N. This can be done by rearranging the expansion (3.1) with equation (3.6)

$$\left.\begin{aligned} &p(X,Y) = P_{-2}(X)\chi_2(Y) + P_{-1}(X)\chi_1(Y) + \sum_{n\ge 0} P_n(X)\varphi_n(Y), \\ &\text{with} \qquad P_{-i} \equiv a_{iN} p_{-i} \text{ and } P_{n\ge 0} \equiv p_n - \chi_{1n} P_{-1} - \chi_{2n} P_{-2}, \end{aligned}\right\} \tag{4.3}$$

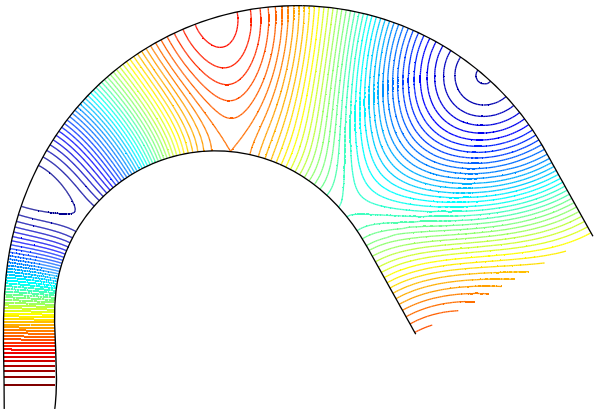

Figure 2. Contour of the real part of the pressure field in a 'trunk' as defined by equations (4.4). A plane wave with frequency $kh_0 = 0.75$ enters the waveguide at the narrow side, of width h_0. (Online version in colour.)

as written in [14–16], and the new P_n is the general term of the series in the IMM (see also appendix B*a*). Thus, the convergence of the wavefield is given by the highest error between the error of the modal components and the error of the remaining series. On the contrary, the convergence of ϵ_N^R is not concerned by the remaining series but only by the error on the modal component $\|p_0^N - p_0^e\|$ owing to the truncation. It follows that R has a convergence equal to or better than that of the wavefield.

(iii) Finally, to be consistent when we compare the two methods, MM and IMM, the number of accounted modes, denoted N_m, has to be the same. Thus, in the MM, $N = N_\mathrm{m}$ is the number of Neumann modes in the expansion, and in the IMM the truncation is $N = N_\mathrm{m} - 2$, plus the two supplementary modes.

(a) The elephant's trunk

First, a validation is presented by considering the same 'elephant's trunk' geometry as in [12] (figure 2), which connects two straight ducts with widths h_0 and $4h_0$, respectively, and is parametrized as follows:

$$\kappa(X) = \begin{cases} 0 & \text{if } X \le 0, \\ \dfrac{0.2}{h_0} & \text{if } 0 < X < L, \\ 0 & \text{if } X \ge L, \end{cases} \tag{4.4a}$$

and

$$h_2(X) = -h_1(X) = \begin{cases} \dfrac{h_0}{2} & \text{if } X \le 0, \\ \left[1 + 9\left(\dfrac{X}{L}\right)^3 - 6\left(\dfrac{X}{L}\right)^3\right]\dfrac{h_0}{2} & \text{if } 0 < X < L, \\ 2h_0 & \text{if } X > L. \end{cases} \tag{4.4b}$$

As in [12], we choose $L = 3.27h_0$. Figure 2 shows the real part of the wavefield obtained with a plane incident wave with frequency $kh_0 = 0.75$. At this frequency, only one mode is propagating. In figure 3, the improvement in the convergences using the IMM is illustrated ($N_e = 100$ has been used for the reference solutions, for which the results of the IMM differ by $10^{-2}\%$ from the result of the MM). The same tendency as that reported in [13,17] is observed: the rate of decay of the general term of the series is increased from $1/n^2$ in the MM to $1/n^4$ in the IMM (figure 3*a*). This leads to an accelerated convergence of the modal series, resulting in an error ϵ_N on the wavefield

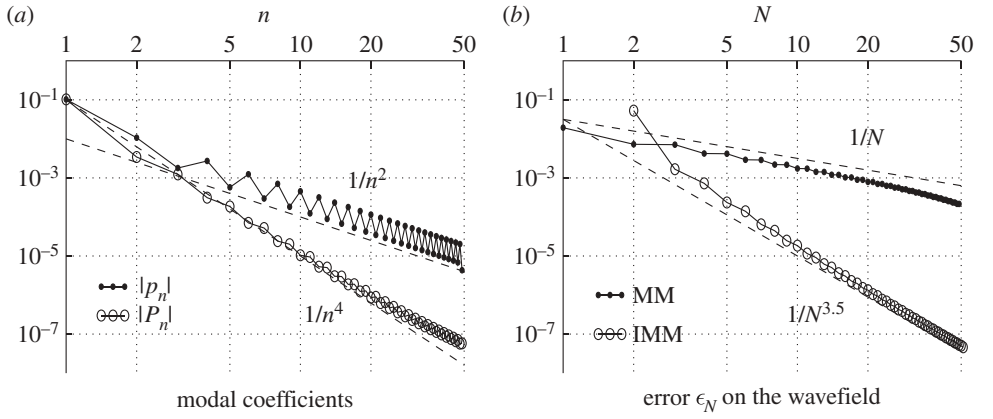

Figure 3. Convergence of the wavefield in the geometry of the elephant's trunk. (*a*) Rate of decay of the general term of the remaining series, $|p_n|$ in the classical MM and $|P_n|$, equation (4.3), in the IMM. (*b*) Error ϵ_N, equation (4.1), as a function of the order of truncation N in the MM (closed symbols) and in the IMM (open symbols).

from $1/N$ to about $1/N^{3.5}$ (figure 3*b*), that is, the highest expected convergence (owing to the remaining series).

Figure 4 shows the results for the reflection coefficient R, whose variation as a function of the non-dimensional frequency kh_0/π is shown in figure 4*b* in the range $kh_0 \in [0, 3\pi/4]$ (the number of propagating modes, N_p, at the output of the waveguide varies from $N_\mathrm{p} = 1$ to $N_\mathrm{p} = 3$). The superconvergence, which we already observed in [13] for a waveguide with one varying wall, is recovered here: the relative error ϵ_N^R decays as $1/N$ in the MM and as about $1/N^{5.5}$ in the IMM ($1/N^{4.5}$ was observed in [13]).

This superconvergence is of great interest for the efficiency of the numerical method and this is illustrated in figure 4*c*. In the MM, taking into account the 2 or 3 first evanescent modes in addition to the N_p propagating modes ($N_\mathrm{m} = N_\mathrm{p} + 2$ or $N_\mathrm{p} + 3$) does not change significantly the accuracy in the determination of R (dotted lines): in the presented example, about 4% on average in the whole range of frequency. In the IMM, we have considered the same N_m values, which means that we accounted only for the propagating modes ($N = N_\mathrm{p}$) and the two degrees of freedom are the two supplementary modes, leading to $N_\mathrm{m} = N_\mathrm{p} + 2$, or we accounted for the first evanescent mode, $N = N_\mathrm{p} + 1$, $N_\mathrm{m} = N_\mathrm{p} + 3$. The result is excellent and quite intuitive: when no evanescent mode is taken into account (black solid curve), the accuracy in R is better in the IMM than in the MM, except near the cut-off frequencies where, precisely, the weight of the mode passing from evanescent to propagating becomes significant. As soon as the first evanescent mode is taken into account (red solid curve), the error on R is decreased by at least one order of magnitude (0.1% on average in the whole range of frequency).

(b) The serpent billiard

In the previous example, we have confirmed that the modal formulation with two supplementary modes reaches a better convergence than the classical formulation. This was our first goal. Here, we explore the role of these supplementary modes with respect to the boundary conditions at the wall of the bent guide, and the consequences, if any, on the convergence. To do that, we consider the geometry of the so-called 'serpent billiard' (because of its particular properties in quantum chaos [28]). In the present case, we are only interested in its shape: the serpent billiard is built as a succession of semicircular rings of radii r and R for the inner and outer circular arcs, respectively, connecting two straight ducts of width $(R - r)$ (figure 5). This geometry can be parametrized using two geometrical transformations, called A and B (two curves $\mathbf{OS_0}(X)$; figure 1), leading to different multi-modal formulations. In the A-transformation, the Neumann modes used in

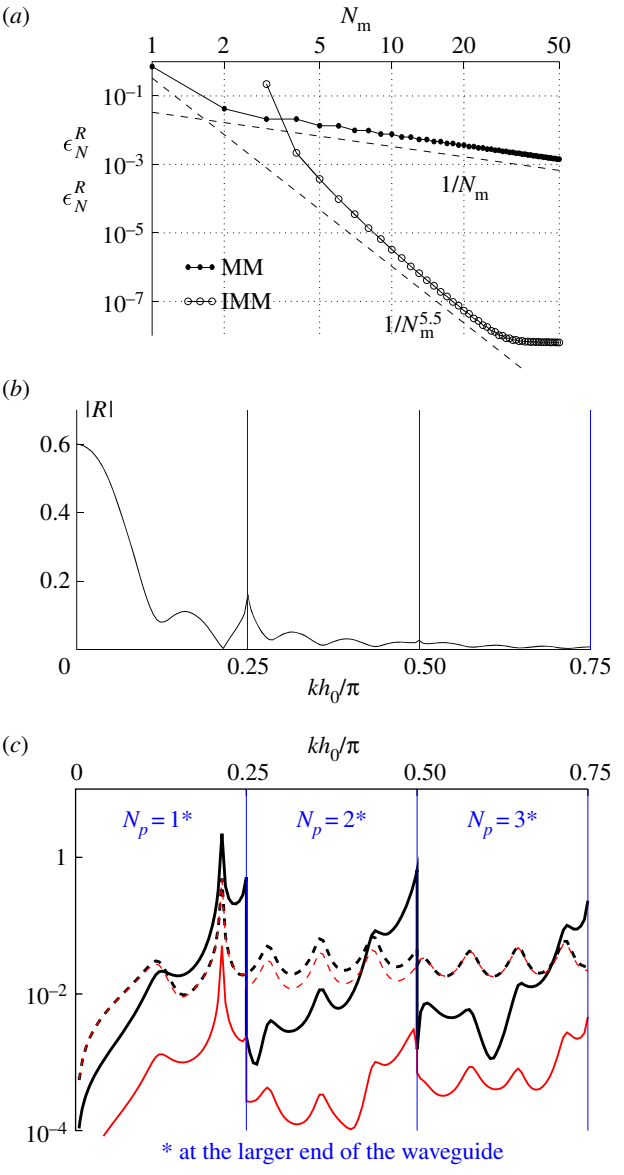

Figure 4. (*a*) Convergence of the reflection coefficient R, ϵ_N^R, as a function of the truncation N_m. (*b*) Reflection coefficient R at the entrance of the 'trunk' waveguide, computed with $N_m = 50$ (reference calculation), as a function of the non-dimensional frequency kh_0/π. (*c*) Relative errors on R, for $N_m = N_p + 2$ (thick black curves) and $N_m = N_p + 3$ (thin red curves), with the MM (dashed curves) and with the IMM (solid curves). (Online version in colour.)

the MM do not satisfy the right boundary conditions, whereas in the B-transformation they do. As previously stated, we address here the question of the link between the behaviour of the computed solution at the boundary and the convergence of the method.

(i) The A-transformation

Because the two terminal ducts have the same direction, the serpent shape can be seen as a guide with zero curvature, $\kappa(X) = 0$, and two varying walls, $h_1(X)$ and $h_2(X)$ (as in [17]). The A-transformation is such that $X = x$, $Y = (y - h_1)/h$, with $h = h_1 + h_2$.

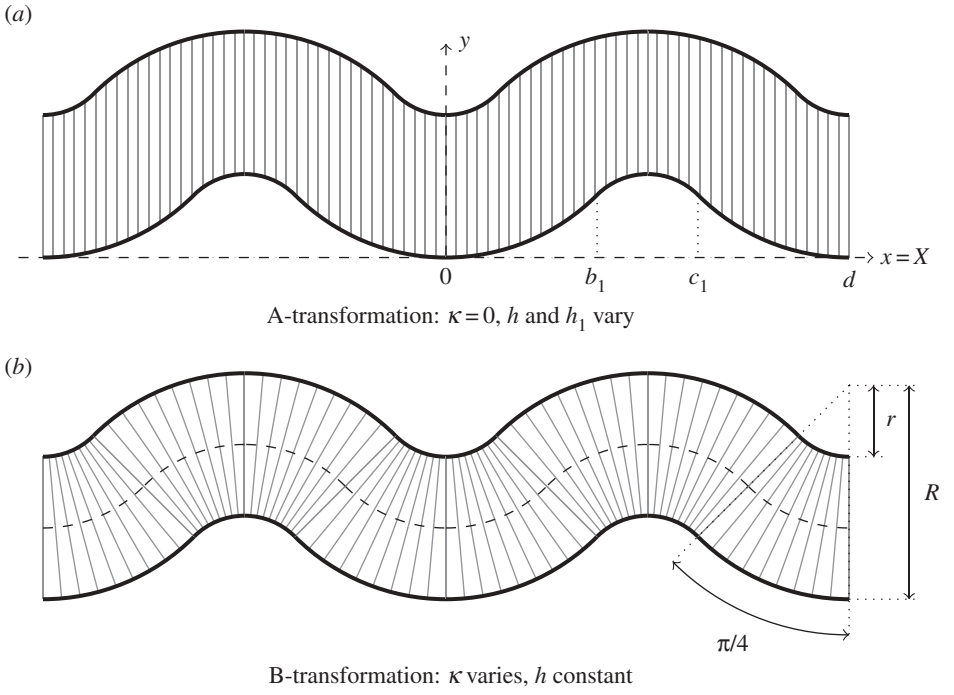

Figure 5. Iso lines $X =$ constant for the two transformations; the dotted line indicates $\mathbf{OS}_0(X)$. (*a*) The A-tranformation, with zero curvature and two varying walls; (*b*) the B-transformation with varying (piecewise constant) curvature and constant transverse height.

As N_c is the number of periodic cells of the serpent, $L = N_c d$, with $d \equiv \sqrt{2}(R + r)$, is the total length of the scattering region. At the inlet and outlet, $X < 0$ and $X > L$, we have $h_1(X) = 0$, $h(X) = (R - r)$. Next, with $Y_c \equiv R - (R + r)/\sqrt{2}$, the basic cell of the serpent is described by $h(X) = h_1(X) - h_2(X)$, with

$$h_1(X) = \begin{cases} R - \sqrt{R^2 - X^2}, & \text{if } 0 \le X < b_1 \equiv \dfrac{R}{\sqrt{2}}, \\ Y_c + \sqrt{r^2 - \left(X - \dfrac{d}{2}\right)^2}, & \text{if } b_1 \le X < c_1 \equiv b_1 + \sqrt{2}r, \\ R - \sqrt{R^2 - (X - d)^2}, & \text{if } c_1 \le X < d \end{cases} \tag{4.5a}$$

and

$$h_2(X) = \begin{cases} R - \sqrt{r^2 - X^2}, & \text{if } 0 \le X < b_2 \equiv \dfrac{r}{\sqrt{2}}, \\ Y_c + \sqrt{R^2 - \left(X - \dfrac{d}{2}\right)^2}, & \text{if } b_2 \le X < c_2 \equiv b_2 + \sqrt{2}R, \\ R - \sqrt{r^2 - (X - d)^2}, & \text{if } c_2 \le X < d, \end{cases} \tag{4.5b}$$

and the next cells (if there are any) are deduced by shifting the origin $X \to X + d$; in the presented case, two cells are considered.

Figure 6 shows the real part of the computed wavefield in the classical MM and in the IMM. At frequency $k(R - r) = 1$, one mode is propagating and we have used $N_m = 4$ modes in each formulation. As expected, without the boundary mode, the MM suffers from spurious oscillations near the walls (Gibbs phenomenon). Next, the observations are similar to the case of the trunk (results are not reported): the rate of convergence ϵ_N is increased from $1/N$ for the MM to $1/N^{3.5}$

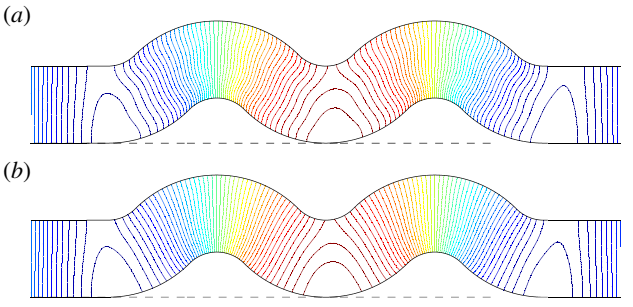

Figure 6. Contour of the real part of the pressure field in the serpent geometry. The wavefields have been computed using the A-transformation (leading to equations (4.5)); the dotted line indicates $\mathbf{OS_0}(X)$ in this transformation. A plane wave with frequency $k(R-r)=1$ enters the waveguide from the left. (*a*) In the MM with $N=4$ and (*b*) in the IMM with $N=2$; in both cases $N_\mathrm{m}=4$ modes are used in the expansions. (Online version in colour.)

for the IMM and the superconvergence of the reflection coefficient is observed, from $1/N$ to $1/N^{4.5}$ (this increase in the convergence is the same as that observed in [13] and differs slightly from the convergence $1/N^{5.5}$ observed for the trunk).

Let us now focus on the behaviour of the computed solution at the walls. The boundary conditions on the lower ($Y=0$) and upper ($Y=1$) walls are, from equation (2.9), $\partial_n p_{|\mathrm{lower}} = \partial_n p_{|\mathrm{upper}} = 0$, with

$$\left.\begin{aligned} &\partial_n p_{|\mathrm{lower}} = \partial_Y p(X,0) - h_1'(X) q(X,0) \\ \text{and}\quad &\partial_n p_{|\mathrm{upper}} = \partial_Y p(X,1) - [h'(X) + h_1'(X)] q(X,0). \end{aligned}\right\} \tag{4.6}$$

The modal components (q_n) have been computed, in addition to the (p_n), in the MM and in the IMM, and the above quantities have been calculated. Results are reported in figure 7; in both cases, the boundary conditions are not satisfied. However, in the MM, $\partial_n p_{|\mathrm{wall}}$ remains $O(h')$ for any truncation. On the contrary, in the IMM, these quantities vanish asymptotically for large N with a rate of decay $1/N^2$. In the present case, the introduction of the supplementary modes tends to restore the right boundary condition, and they merit their name of 'boundary modes'.

(ii) The B-transformation

The B-transformation uses a curve $\mathbf{OS_0}(X)$, being the middle line in the inlet and outlet ducts and being a succession of semicircular arcs of radius $R_m \equiv (r+R)/2$. It follows that $h_1(X) = -(R-r)/2$ and $h(X) = (R-r)$ are constant. The curvature $\kappa(X) = 0$ in the inlet and outlet ($X<0$ and $X>L_s$, with $L_s = N_\mathrm{c} R_m \pi$ the total arc length) and

$$\kappa(X) = \begin{cases} -\dfrac{1}{R_m}, & \text{if } 0 \le \dfrac{X}{R_m} < \dfrac{\pi}{4}, \text{ or if } \dfrac{3\pi}{4} \le \dfrac{X}{R_m} < \pi, \\ \dfrac{1}{R_m}, & \text{if } \dfrac{\pi}{4} \le \dfrac{X}{R_m} < \dfrac{3\pi}{4}. \end{cases} \tag{4.7}$$

The next cells are deduced by shifting the origin $X \to X + R_m\pi$.

Figure 8 shows the wavefields computed in the MM and IMM using $N_\mathrm{m}=4$. In this case, with h_1 and h constant, the condition to be satisfied by the wavefield $p(X,Y)$ at the walls is $\partial_Y p(X, Y=0) = \partial_Y p(X, Y=1) = 0$, from equation (2.9). This means that the usual Neumann modes $\varphi_{n\ge 0}$, used in the MM, satisfy the right boundary condition and one expects that it is the best choice to expand the solution.

This is the question that we address now: when the Neumann basis is well adapted to account for the boundary conditions, does the use of supplementary modes improve or degrade the convergence of the computed solution?

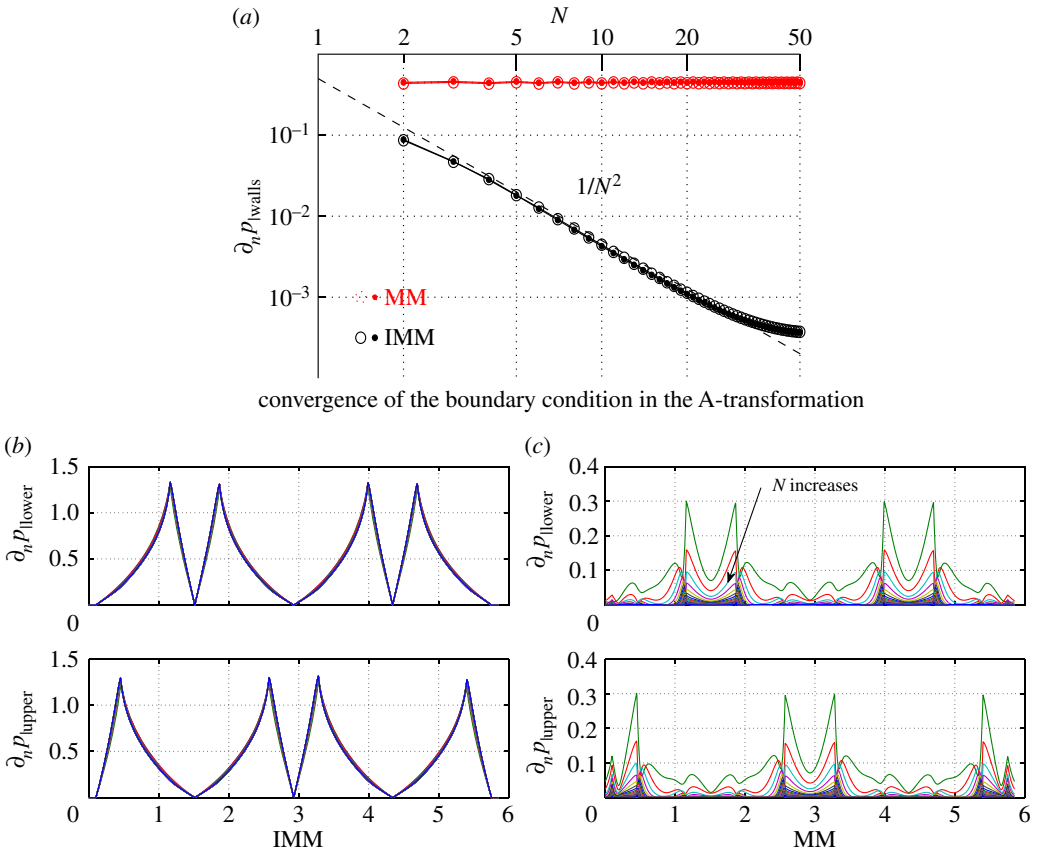

Figure 7. (*a*) Rates of decay of $\| \partial_n p_{|\text{walls}} \|$, lower $Y = 0$ and upper $Y = 1$, as a function of the truncation N. (*b*,*c*) Profiles of $\partial_n p_{|\text{walls}}$, as a function of X for increasing N values (the set of curves collect $N = 1$–50) (*b*) in the IMM and (*c*) in the MM. (Online version in colour.)

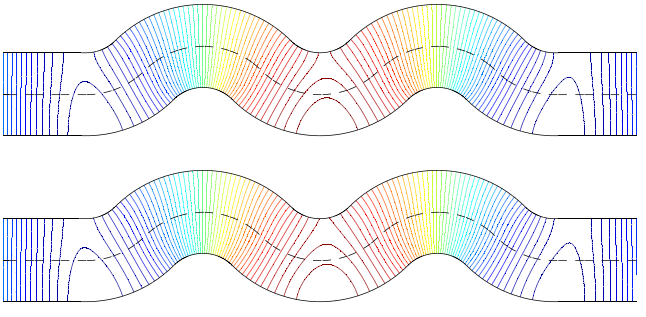

Figure 8. Same representation as in figure 6. The wavefields have been computed using the B-transformation (leading to equations (4.7)). (Online version in colour.)

Consider first the behaviour of the solution at the walls. While $\partial_n p_{|\text{walls}}$ vanish for any truncation in the MM, by construction, their values in the IMM are

$$\left.\begin{aligned} \partial_n p_{|\text{lower}} &= \partial_Y p(X,0) = \frac{\pi}{2}[a_{1N} a_1 p_{-1}(X) - a_{2N} a_2 p_{-2}(X)] \\ \text{and} \qquad \partial_n p_{|\text{upper}} &= \partial_Y p(X,1) = -\frac{\pi}{2}[a_{1N} a_1 p_{-1}(X) + a_{2N} a_2 p_{-2}(X)], \end{aligned}\right\} \tag{4.8}$$

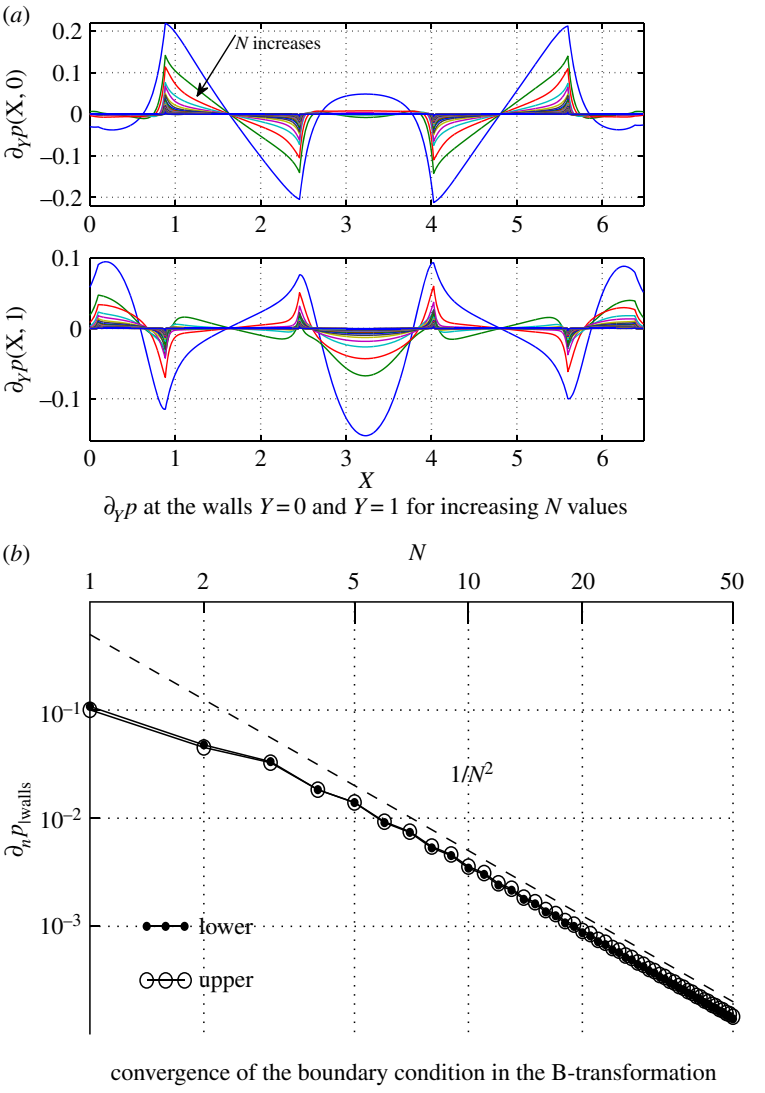

Figure 9. (*a*) Profiles of $\partial_Y p_{|\text{walls}} = \partial_Y p(X, Y = 0, 1)$ as a function of X for increasing N values (the set of curves collect $N = 1$–50). (*b*) Rates of decay of $\| \partial_Y p(X, Y = 0, 1) \|$ as a function of the truncation N. (Online version in colour.)

and the corresponding profiles are plotted as a function of X for increasing truncation N in figure 9*a*. The right boundary condition is violated in the IMM, and, as in the case of the trunk, it is restored asymptotically only, for large N (figure 9*b*). Clearly, in the present case, the supplementary modes degrade the behaviour of the solution at the walls.

Consider now the problem of convergence. We have checked that the general terms of the remaining series p_n and P_n both have a rate of decay $1/n^4$ (results are not reported) so that the highest expected convergence is $1/N^{7/2}$. Figure 10 shows the convergences of the wavefield, ϵ_N, and of the reflection coefficients, ϵ_N^R.

In the MM, $\epsilon_N \propto 1/N^3$, as already observed in [12], indicating that the error is attributable to the error on the modal components. The result of this is that the error on the reflection coefficient behaves the same, $\epsilon_N^R \propto 1/N^3$.

In the IMM, on the contrary, $\epsilon_N \propto 1/N^{3.5}$ reaches the convergence of the remaining series, which indicates that the error on the modal components is equal or smaller. The error of the remaining series does not affect the error on the scattering coefficients, and we find $\epsilon_N^R \propto 1/N^{4.5}$.

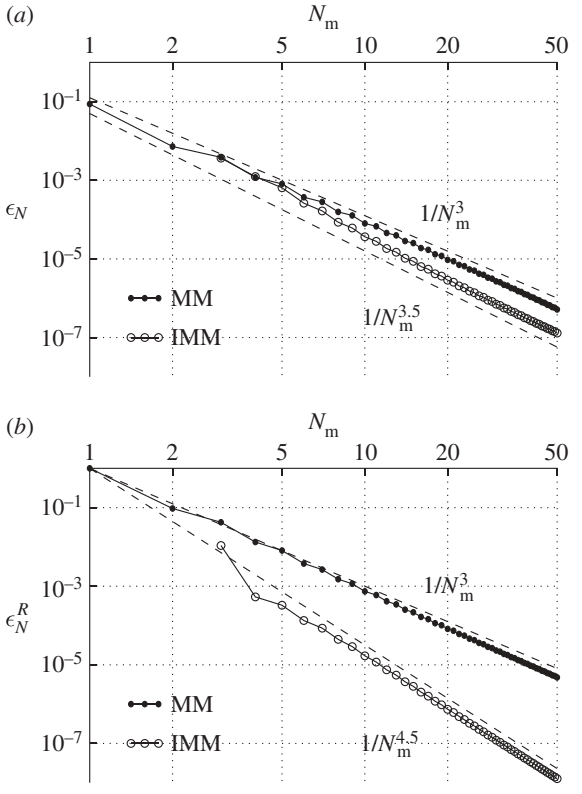

Figure 10. Convergences in the geometry of the serpent using the B-tranformation. (*a*) The error on the wavefield ϵ_N as a function of the truncation N and (*b*) the error on the reflection coefficients ϵ_N^R, in the MM (filled symbols) and in the IMM (open symbols).

This result was not expected *a priori* and we have no proof that it is a general result. However, it indicates that the role of the supplementary modes is more complex than the improvement of the behaviour of the solution with respect to the boundary conditions. In general, the link between the ability of the series representation of the solution to satisfy the right boundary condition and the convergence of this solution is not trivial, and there is a lack of theoretical predictions, for instance concerning the error on the modal components.

In the presented examples, we have observed that for the A-transformation

$$\left.\begin{aligned} &\partial_n p(x,\text{wall}) \neq 0, \quad \text{in the MM} \\ \text{and} \quad &\partial_n p(x,\text{wall}) \to 0, \quad \text{asymptotically } \left(\frac{1}{N^2}\right) \text{ in the IMM,} \end{aligned}\right\} \tag{4.9}$$

and the resulting computational efficiency of the IMM is significantly increased. For the B-transformation,

$$\left.\begin{aligned} &\partial_n p(x,\text{wall}) = 0, \quad \text{in the MM} \\ \text{and} \quad &\partial_n p(x,\text{wall}) \to 0, \quad \text{still asymptotically } \left(\frac{1}{N^2}\right) \text{ in the IMM,} \end{aligned}\right\} \tag{4.10}$$

and, although less significant, the use of supplementary modes does improve the computational efficiency of the method.

5. Conclusion

We have presented an efficient multi-modal method for the propagation of acoustic waves in bent guides with variable cross section. Technically, a key feature of the present method is the use of a flexible geometrical transformation, which allows for a wide variety of waveguide geometries, including variable or piecewise constant curvature. In addition, an improved version of the MM has been presented, reaching a high computational efficiency. Following previous work [13–17], this has been done by means of a truncated modal basis enriched with two supplementary modes. In most cases, the improvement in the convergences is impressive, from $1/N$ to $1/N^{3.5}$ on the wavefield and from $1/N$ to typically $1/N^5$ (with some variability) when considering the scattering coefficients. As previously stated [13], this superconvergence of the scattering coefficients is of practical interest. Indeed, one is often more interested in the scattering properties of the non-uniform parts in the guide than in the details of the wavefield pattern inside those regions.

Another, and related, question that has been addressed is the role of the supplementary modes. Originally, they were introduced in order to build a series representation of the field able to better account for the right boundary condition at the walls $\partial_n p_{|\text{wall}} = 0$, when it is not satisfied by the usual Neumann modes. In most cases, the Neumann modes violate the boundary condition because of the curvature and variable cross section; then, the supplementary modes have been shown to restore the right boundary condition asymptotically, and this is accompanied by an improved convergence. More surprisingly, we have shown that an improved convergence is also obtained when the Neumann modes satisfy the right boundary condition; however, in this case, the supplementary modes degrade the solution at the boundary. Similar conclusions in the case of guides with local Robin boundary conditions are reported in [18]. On the one hand, this raises the question of the role of the supplementary modes and the link between the convergence of the truncated series and their ability to satisfy the boundary conditions. On the other hand, this paves the way towards the use of supplementary modes in a wide range of scattering problems.

Funding statement. The authors acknowledge the financial support of the French National Agency (ANR), within the framework of project ProCoMedia, ANR-10-INTB-0914.

Appendix A. Properties of the numerical scheme: reciprocity and energy conservation

Because the initial problem satisfies the properties of reciprocity and of energy conservation, it is of importance to check that our modal formulation preserves them.

Reciprocity can be translated in the following property: if $p_A(x,y)$ and $p_B(x,y)$ are two solutions to the scattering problem, then $\int [p_A(x,y)\nabla p_B(x,y)\cdot\mathbf{N} - p_B(x,y)\nabla p_A(x,y)\cdot\mathbf{N}]\,\mathrm{d}S = 0$, and the integral is performed on any closed surface in the waveguide. Equivalently, in the (X,Y) coordinates, reciprocity reads, from equation (2.3),

$$\int \mathrm{d}S[p_A(X,Y)\mathtt{H}\nabla p_B(X,Y) - p_B(X,Y)\mathtt{H}\nabla p_A(X,Y)]\cdot\mathbf{N} = 0,$$

with $\mathtt{H} \equiv {}^t\mathtt{J}\mathtt{J}/\det\mathtt{J}$. Next, one considers for this surface the boundary waveguide segment between X and $X + \mathrm{d}X$. It is easy to see that

$$\mathtt{H}\nabla p(X,Y) = \begin{pmatrix} q(X,Y) \\ 0 \end{pmatrix},$$

and the Y-component vanishes because of the boundary condition (vanishing normal derivative) $\nabla p(x,y)\cdot\mathbf{N} = 0$ at the walls, leading to equation (2.9). Thus, reciprocity imposes that $\int \mathrm{d}Y\,[p_A q_B - p_B q_A]$ is independent of X. This translates in terms of the vectors of modal components

$$\partial_X[\,{}^t\mathbf{p}_A\mathbf{q}_B - {}^t\mathbf{p}_B\mathbf{q}_A] = 0.$$

It is now sufficient to use equation (3.3), written formally

$$\frac{\mathrm{d}}{\mathrm{d}X}\begin{pmatrix}\mathbf{p}\\ \mathbf{q}\end{pmatrix}=\begin{pmatrix}\mathtt{a} & \mathtt{b}\\ \mathtt{c} & \mathtt{d}\end{pmatrix}\begin{pmatrix}\mathbf{p}\\ \mathbf{q}\end{pmatrix}, \tag{A 1}$$

to get

$${}^t\mathbf{p}_B({}^t\mathtt{a}+\mathtt{d})\mathbf{q}_A-{}^t\mathbf{p}_A({}^t\mathtt{a}+\mathtt{d})\mathbf{q}_B+{}^t\mathbf{q}_A(\mathtt{b}-{}^t\mathtt{b})\mathbf{q}_B-{}^t\mathbf{p}_A(\mathtt{c}-{}^t\mathtt{c})\mathbf{p}_B=0.$$

From equation (3.3), we have $\mathtt{d}=-{}^t\mathtt{a}$ and the matrices $\mathtt{b}$ and $\mathtt{c}$ are symmetric (real), from which the above relation is verified.

The energy conservation concerns $p_A=p$ and $p_B=\bar{p}$, leading to the conservation, along X, of the Poynting vector $\Pi=\mathrm{Im}[{}^t\bar{\mathbf{p}}\mathbf{q}]$. The matrices $(\mathtt{a},\mathtt{b},\mathtt{c},\mathtt{d})$ being real, the energy conservation simply follows from the reciprocity.

Appendix B. Numerical implementation using the admittance matrix

The difficulties in numerically solving equation (3.3) (we use in this section the formal representation (A 1)) are known and they have been solved in a series of papers using the so-called admittance matrix [3,11,12]. Here, we recall the principles of the numerical scheme. First, the admittance matrix $\mathtt{Y}$ is defined as $\mathbf{q}=\mathtt{Y}\mathbf{p}$. Using (A 1) the admittance matrix satisfies a Riccati equation,

$$\mathtt{Y}'=-\mathtt{Y}\mathtt{b}\mathtt{Y}+\mathtt{d}\mathtt{Y}-\mathtt{Y}\mathtt{a}+\mathtt{c}, \tag{B 1}$$

that can be solved numerically from the output ($X=L$) to the input ($X=0$) of the region of interest, given an initial condition $\mathtt{Y}(L)$. As the region $X>L$ is such that only right-going waves can propagate (straight terminations with constant height are assumed), then $\mathtt{a}(x>L)=\mathtt{d}(x>L)=\mathtt{0}$, $\mathtt{b}(x>L)=\mathtt{I}/h$ and $\mathtt{c}=\mathtt{K}^2/h$. Thus, the Riccati equation has a constant solution for $x>L$ and $\mathtt{Y}(L)=\mathtt{K}$. This is the key point of the presented formulation: the IMM, as the classical MM, has been built to leave the modes uncoupled in the straight parts of the waveguides. If this were not the case, one would have been unable to define a consistent initial condition $\mathtt{Y}(L)$.

Once the admittance matrix has been calculated along the X-axis, the modal wavefield $\mathbf{p}$ can be calculated as the solution of the first-order, numerically stable, equation

$$\mathbf{p}'=[\mathtt{a}+\mathtt{b}\mathtt{Y}]\mathbf{p},$$

from the input to the output, given an initial condition $\mathbf{p}(0)$, which accounts for the source condition (for MMs, as the one way method, more adapted to long waveguides; see also [21]).

(a) On the calculation of the error

In the case of the IMM formulation, we look for an expression of the error on the wavefield,

$$\epsilon_N\equiv\frac{\|p^N-p^e\|}{\|p^e\|}, \tag{B 2}$$

that avoids the integral over y (because these integrals need more and more discretization along y for increasing N values, it is a source of error in the estimate of ϵ). The difficulty here is that the expansion of p^N involves φ_{-i}, $i=1,2$ that are non-orthogonal to the $\varphi_{n\geq N}$ present in the expansion of p^e. To begin with, we use

$$p^N-p^e=\sum_{i=1,2}[p^e_{-i}\varphi^e_{-i}-p_{-i}\varphi_{-i}]+\sum_{n=0}^{N-1}(p^e_n-p^N_n)\varphi_n+\sum_{n=N}^{N_e}p^e_n\varphi_n \tag{B 3}$$

to define the remaining series RS, obtained when neglecting the variation of the modal component p^N_n with N, that is, assuming $p_n=p^N_n=p^e_n$. We get

$$\mathrm{RS}=\sum_{i=1,2}p_{-i}[\varphi^e_{-i}-\varphi_{-i}]+\sum_{n=N}^{N_e}p_n\varphi_n, \tag{B 4}$$

from which we define the general term of the remaining series

$$P_{-i} \equiv a_{iN} p_{-i} \quad \text{and} \quad P_{n\geq 0} \equiv p_n - \chi_{1n} P_{-1} - \chi_{2n} P_{-2} \tag{B 5}$$

to get $\mathrm{RS} = \sum_{n=N}^{N_e} P_n \varphi_n$. Coming back to the error as a function of P_n

$$p^N - p^e = \sum_{i=1,2} [P^e_{-i} - P^N_{-i}]\chi_i + \sum_{n=0}^{N-1} (P^e_n - P^N_n)\varphi_n + \sum_{n=N}^{N_e} P^e_n \varphi_n, \tag{B 6}$$

we obtain the estimation of the error, with

$$\begin{aligned} \|p^N - p^e\|^2 = {} & \sum_{n=-2}^{N-1} \int \mathrm{d}x |P^e_n - P^N_n|^2 + \sum_{n=N}^{N_e} \int \mathrm{d}x |P^e_n|^2 \\ & + 2\,\mathrm{Re}\left\{ \sum_{i=1,2} \int \mathrm{d}x (P^e_{-i} - P^N_{-i})^* \left[\sum_{n=0}^{N-1} \chi_{in} (P^e_n - P^N_n) + \sum_{n=N}^{N_e} \chi_{in} P^e_n \right] \right\}, \end{aligned} \tag{B 7}$$

where star * denotes the complex conjugate. This is the above expression, together with

$$\|p^e\|^2 = \sum_{n=-2}^{N_e} \int dx |P^e_n|^2 + 2\,\mathrm{Re}\left\{ \sum_{i=1,2} \int dx P^e_{-i}{}^* \sum_{n=0}^{N_e} \chi_{in} (P^e_n) \right\}, \tag{B 8}$$

that is used to compute the errors in the presented results.

Appendix C. Matrices

We give here the expressions of the matrices C, D, E and F.

(a) Modal method

For $(m, n) \in [0, N-1]^2$,

$$\left.\begin{aligned} \mathtt{C}_{mn} \equiv (Y\varphi_m, \varphi_n) &= \begin{cases} \dfrac{1}{2} & \text{if } m = n, \\ \dfrac{\sqrt{2-\delta_{m0}}\sqrt{2-\delta_{n0}}}{\pi^2} [(-1)^{m+n} - 1] \dfrac{(m^2+n^2)}{(m^2-n^2)^2} & \text{otherwise,} \end{cases} \\ \mathtt{D}_{mn} \equiv (Y\varphi'_m, \varphi'_n) &= \begin{cases} \dfrac{n^2\pi^2}{2} & \text{if } m = n, \\ [(-1)^{m+n} - 1] \dfrac{4m^2n^2}{(m^2-n^2)^2}, & \text{otherwise,} \end{cases} \\ \mathtt{E}_{mn} \equiv (Y\varphi_m, \varphi'_n) &= \begin{cases} \dfrac{1-\delta_{m0}}{2} & \text{if } m = n, \\ \sqrt{2-\delta_{m0}}\sqrt{2-\delta_{n0}} (-1)^{m+n} \dfrac{n^2}{n^2-m^2} & \text{otherwise} \end{cases} \end{aligned}\right\} \tag{C 1}$$

and

$$\mathtt{F}_{mn} \equiv (\varphi_m, \varphi'_n) = \begin{cases} 0 & \text{if } m = n, \\ \sqrt{2-\delta_{m0}}\sqrt{2-\delta_{n0}} [(-1)^{m+n} - 1] \dfrac{n^2}{n^2-m^2} & \text{otherwise.} \end{cases}$$

(b) Improved modal method

The scalar products $\chi_{in} \equiv (\varphi_n, \chi_i)$ are, for $n \in [0, N-1]$ and $i = 1, 2$,

$$\chi_{in} = \frac{a_i}{2}[(-1)^n + \epsilon_i]\alpha_n, \tag{C 2}$$

with $\epsilon_1 = 1$, $\epsilon_2 = -1$, $a_i = 1/\sqrt{1 + \epsilon_i 2/\pi}$ and

$$\alpha_n = -\frac{\sqrt{2 - \delta_{n0}}}{\pi}\frac{4}{4n^2 - 1}. \tag{C 3}$$

The supplementary terms in the matrices $\mathtt{C}$, $\mathtt{D}$, $\mathtt{E}$ and $\mathtt{F}$ owing to the boundary modes can be written in the generic form

$$\left.\begin{aligned} &\mathtt{M}_{m,-i} = a_{iN}\left(\mathtt{m}_{m,-i} - \sum_{n=0}^{N-1}\chi_{in}\mathtt{M}_{mn}\right), \quad \mathtt{M}_{-i,n} = a_{iN}\left(\mathtt{m}_{-i,n} - \sum_{m=0}^{N-1}\chi_{im}\mathtt{M}_{mn}\right) \\ \text{and} \quad &\mathtt{M}_{-i,-j} = a_{iN}a_{jN}\left(\mathtt{m}_{-i,-j} - \sum_{n=0}^{N-1}\chi_{jn}\mathtt{m}_{-i,n} - \sum_{m,n=0}^{N-1}\chi_{im}[\mathtt{m}_{m,-j} - \chi_{jn}\mathtt{M}_{mn}]\right), \end{aligned}\right\} \tag{C 4}$$

where $\mathtt{M}$ stands for $\mathtt{C}$, $\mathtt{D}$, $\mathtt{E}$ or $\mathtt{F}$ and $\mathtt{m}$ stands for $\mathtt{c}$, $\mathtt{d}$, $\mathtt{e}$, $\mathtt{f}$, given in the following.

(i) Matrix C

Defining

$$\left.\begin{aligned} &\mathtt{c}_m^+ \equiv \sqrt{2 - \delta_{m0}}\int_0^1 \mathrm{d}Y Y \cos m\pi Y \cos\frac{\pi Y}{2} = \frac{\sqrt{2 - \delta_{m0}}}{2\pi}\left(\frac{4(-1)^m}{4m^2 - 1} + \frac{8}{\pi}\frac{4m^2 + 1}{(4m^2 - 1)^2}\right) \\ \text{and} \quad &\mathtt{c}_m^- \equiv \sqrt{2 - \delta_{m0}}\int_0^1 \mathrm{d}Y Y \cos m\pi Y \sin\frac{\pi Y}{2} = \frac{\sqrt{2 - \delta_{m0}}}{2\pi}8(-1)^m\frac{4m^2 + 1}{(4m^2 - 1)^2}, \end{aligned}\right\} \tag{C 5}$$

we have

$$\left.\begin{aligned} &\mathtt{c}_{-1,m} = a_1[\mathtt{c}_m^+ + \mathtt{c}_m^-], \quad \mathtt{c}_{-2,m} = a_2[\mathtt{c}_m^+ - \mathtt{c}_m^-] \\ \text{and} \quad &\mathtt{c}_{-1,-1} = a_1^2\left(\frac{1}{2} + \frac{1}{\pi}\right), \quad \mathtt{c}_{-2,-2} = a_2^2\left(\frac{1}{2} - \frac{1}{\pi}\right), \quad \mathtt{c}_{-1,-2} = -\frac{2a_1a_2}{\pi^2}. \end{aligned}\right\} \tag{C 6}$$

(ii) Matrix D

Defining

$$\left.\begin{aligned} &\mathtt{d}_m^+ \equiv \sqrt{2 - \delta_{m0}}\int_0^1 \mathrm{d}Y Y \sin m\pi Y \cos\frac{\pi Y}{2} = -\frac{\sqrt{2 - \delta_{m0}}}{2\pi}8\frac{4(-1)^m m}{(4m^2 - 1)^2} \\ \text{and} \quad &\mathtt{d}_m^- \equiv \sqrt{2 - \delta_{m0}}\int_0^1 \mathrm{d}Y Y \sin m\pi Y \sin\frac{\pi Y}{2} = -\frac{\sqrt{2 - \delta_{m0}}}{2\pi}8\left(\frac{(-1)^m m}{4m^2 - 1} + \frac{1}{\pi}\frac{4m}{(4m^2 - 1)^2}\right), \end{aligned}\right\} \tag{C 7}$$

we have

$$\left.\begin{aligned} &\mathtt{d}_{-1,m} = -\frac{m\pi^2}{2}a_1[\mathtt{d}_m^+ - \mathtt{d}_m^-], \quad \mathtt{d}_{-2,m} = \frac{m\pi^2}{2}a_2[\mathtt{d}_m^+ + \mathtt{d}_m^-] \\ \text{and} \quad &\mathtt{d}_{-1,-1} = a_1^2\frac{\pi^2}{4}\left(\frac{1}{2} - \frac{1}{\pi}\right), \quad \mathtt{d}_{-2,-2} = a_2^2\frac{\pi^2}{4}\left(\frac{1}{2} + \frac{1}{\pi}\right), \quad \mathtt{d}_{-1,-2} = \frac{a_1a_2}{2}. \end{aligned}\right\} \tag{C 8}$$

(iii) Matrix E

The matrix E can be written using $\mathsf{c}^{\pm}$ and $\mathsf{d}^{\pm}$

$$\left.\begin{aligned}
&\mathsf{e}_{-1,m} = -m\pi a_1[\mathsf{d}_m^+ + \mathsf{d}_m^-], \quad \mathsf{e}_{m,-1} = \frac{\pi}{2}a_1[\mathsf{c}_m^+ - \mathsf{c}_m^-],\\
&\mathsf{e}_{-2,m} = -m\pi a_2[\mathsf{d}_m^+ - \mathsf{d}_m^-], \quad \mathsf{e}_{m,-2} = -\frac{\pi}{2}a_2[\mathsf{c}_m^+ + \mathsf{c}_m^-],\\
&\mathsf{e}_{-1,-1} = -\frac{a_1^2}{\pi}, \quad \mathsf{e}_{-2,-2} = \frac{a_2^2}{\pi}, \quad \mathsf{e}_{-1,-2} = -\frac{\pi}{2}a_1a_2\left(\frac{1}{2}+\frac{1}{\pi}\right)\\
\text{and}\quad &\mathsf{e}_{-2,-1} = \frac{\pi}{2}a_1a_2\left(\frac{1}{2}-\frac{1}{\pi}\right).
\end{aligned}\right\} \tag{C 9}$$

(iv) Matrix F

Defining

$$\left.\begin{aligned}
&\mathsf{f}_m^a = \sqrt{2-\delta_{m0}}\int_0^1 \mathrm{d}Y \cos m\pi Y \sin\frac{\pi Y}{2} = -\frac{\sqrt{2-\delta_{m0}}}{2\pi}\frac{4}{4m^2-1},\\
&\mathsf{f}_m^b = \sqrt{2-\delta_{m0}}\int_0^1 \mathrm{d}Y \cos m\pi Y \cos\frac{\pi Y}{2} = (-1)^m\mathsf{f}_m^a,\\
&\mathsf{f}_m^c = \sqrt{2-\delta_{m0}}\int_0^1 \mathrm{d}Y \sin m\pi Y \sin\frac{\pi Y}{2} = -\frac{\sqrt{2-\delta_{m0}}}{2\pi}(-1)^m\frac{8m}{4m^2-1}\\
\text{and}\quad &\mathsf{f}_m^d = \sqrt{2-\delta_{m0}}\int_0^1 \mathrm{d}Y \sin m\pi Y \cos\frac{\pi Y}{2} = -(-1)^m\mathsf{f}_m^c,
\end{aligned}\right\} \tag{C 10}$$

we have

$$\left.\begin{aligned}
&\mathsf{f}_{-1,m} = -m\pi a_1[\mathsf{f}_m^c + \mathsf{f}_m^d], \quad \mathsf{f}_{m,-1} = \frac{\pi}{2}a_1[\mathsf{f}_m^b - \mathsf{f}_m^a],\\
&\mathsf{f}_{-2,m} = -m\pi a_2[\mathsf{f}_m^d - \mathsf{f}_m^c], \quad \mathsf{f}_{m,-2} = -\frac{\pi}{2}a_2[\mathsf{f}_m^a + \mathsf{f}_m^b],\\
&\mathsf{f}_{-1,-1} = 0, \quad \mathsf{f}_{-2,-2} = 0, \quad \mathsf{f}_{-1,-2} = -\frac{\pi}{2}a_1a_2\left[1+\frac{2}{\pi}\right] \quad \text{and} \quad \mathsf{f}_{-2,-1} = \frac{\pi}{2}a_1a_2\left[1-\frac{2}{\pi}\right].
\end{aligned}\right\} \tag{C 11}$$

References

1. Collin RE. 1991 *Field theory of guided waves*, 2nd edn. Piscataway, NJ: IEEE Press.
2. Stevenson AF. 1951 General theory of electromagnetic horns. *J. Appl. Phys.* **22**, 1447–1460. (doi:10.1063/1.1699891)
3. Pagneux V, Amir N, Kergomard J. 1996 A study of wave propagation in varying cross-section waveguides by modal decomposition. Part I. Theory and validation. *J. Acoust. Soc. Am.* **100**, 2034–2048. (doi:10.1121/1.417913)
4. Adams SDM, Craster RV, Guenneau S. 2008 Bloch waves in periodic multi-layered waveguides. *Proc. R. Soc. A* **464**, 2669–2692. (doi:10.1098/rspa.2008.0065)
5. Pagneux V, Maurel A. 2006 Lamb wave propagation in elastic waveguides with variable thickness. *Proc. R. Soc. A* **462**, 1315–1339. (doi:10.1098/rspa.2005.1612)
6. Craster RV, Guenneau S, Adams SD. 2009 Mechanism for slow waves near cutoff frequencies in periodic waveguides. *Phys. Rev. B* **79**, 045129. (doi:10.1103/PhysRevB.79.045129)
7. Martin PA, Dalrymple RA. 1994 On the propagation of water waves along a porous-walled channel. *Proc. R. Soc. Lond. A* **444**, 411–428. (doi:10.1098/rspa.1994.0029)
8. Linton CM, McIver P. 2007 Embedded trapped modes in water waves and acoustics. *Wave Motion* **45**, 16–29. (doi:10.1016/j.wavemoti.2007.04.009)
9. Cobelli P, Pagneux V, Maurel A, Petitjeans P. 2011 Experimental study on water-wave trapped modes. *J. Fluid Mech.* **666**, 445–476. (doi:10.1017/S0022112010004222)
10. Popov E, Nevière M. 2000 Grating theory: new equations in Fourier space leading to fast converging results for TM polarization. *J. Opt. Soc. A* **17**, 1773–1784. (doi:10.1364/JOSAA.17.001773)

11. Pagneux V. 2010 Multimodal admittance method in waveguides and singularity behavior at high frequencies. *J. Comput. Appl. Math.* **234**, 1834–1841. (doi:10.1016/j.cam.2009.08.034)
12. Félix S, Pagneux V. 2001 Sound propagation in rigid bends: a multimodal approach. *J. Acoust. Soc. Am.* **110**, 1329–1337. (doi:10.1121/1.1391249)
13. Maurel A, Mercier JF, Pagneux V. 2014 Improved multimodal admittance method in varying cross section waveguides. *Proc. R. Soc. A* **470**, 20130448. (doi:10.1098/rspa.2013.0448)
14. Athanassoulis GA, Belibassakis KA. 1999 A consistent coupled-mode theory for the propagation of small-amplitude water waves over variable bathymetry regions. *J. Fluid Mech.* **389**, 275–301. (doi:10.1017/S0022112099004978)
15. Athanassoulis GA, Belibassakis KA. 2003 Rapidly-convergent local-mode representations for wave propagation and scattering in curved-boundary waveguides. In *Proc. 6th Int. Conf. on Mathematical and Numerical Aspects of Wave Propagation* (*Waves 2003*), *Jyväskylä, Finland, 30 June–4 July 2003*, pp. 451–456. Berlin, Germany: Springer.
16. Hazard C, Lunéville E. 2008 An improved multimodal approach for non-uniform acoustic waveguides. *IMA J. Appl. Math.* **73**, 668–690. (doi:10.1093/imamat/hxn006)
17. Mercier JF, Maurel A. 2013 Acoustic propagation in non-uniform waveguides: revisiting Webster equation using evanescent boundary modes. *Proc. R. Soc. A* **469**, 20130186. (doi:10.1098/rspa.2013.0186)
18. Félix S, Maurel A, Mercier JF. Submitted. Comparison of improved multimodal methods for the propagation in waveguides with finite wall impedance.
19. Dalrymple RA, Kirby JT, Martin PA. 1994 Spectral methods for forward-propagating water waves in conformally-mapped channels. *Appl. Ocean Res.* **16**, 249–266. (doi:10.1016/0141-1187(94)90015-9)
20. Nilsson B. 2002 Acoustic transmission in curved ducts with varying cross-sections. *Proc. R. Soc. Lond. A* **458**, 1555–1574. (doi:10.1098/rspa.2001.0910)
21. Lu YY, Huang J, McLaughlin JR. 2001 Local orthogonal transformation and one-way methods for acoustic waveguides. *Wave Motion* **34**, 193–207. (doi:10.1016/S0165-2125(00)00083-4)
22. Lu YY, Ho PL. 2002 Beam propagation modeling of arbitrarily bent waveguides. *IEEE Photonics Tech. Lett.* **14**, 1698–1700. (doi:10.1109/LPT.2002.804670)
23. Lu YY. 2004 A local orthogonal transform for acoustic waveguides with an internal interface. *J. Comput. Acoust.* **12**, 37–53. (doi:10.1142/S0218396X04002183)
24. Perrey-Debain E, Abrahams ID. 2012 TE mode mixing dynamics in curved multimode optical waveguides. *Commun. Comput. Phys.* **11**, 525–540.
25. Félix S, Pagneux V. 2004 Sound attenuation in lined bends. *J. Acoust. Soc. Am.* **116**, 1921–1931. (doi:10.1121/1.1788733)
26. Belibassakis KA, Athanassoulis GA. 2002 Extension of second-order Stokes theory to variable bathymetry. *J. Fluid Mech.* **464**, 35–80. (doi:10.1017/S0022112002008753)
27. Athanassoulis GA, Belibassakis KA. 2007 A coupled-mode method for non-linear water waves in general bathymetry with application to steady travelling solutions in constant, but arbitrary, depth. *Discrete Contin. Dynam. Systems Suppl.* **2007**, 75–84.
28. Horvat M, Prosen T. 2004 Uni-directional transport properties of a serpent billiard. *J. Phys. A* **37**, 3133–3145. (doi:10.1088/0305-4470/37/9/006)